INTERNATIONAL JOURNAL OF OPTIMIZATION IN CIVIL ENGINEERING
Int. J. Optim. Civil Eng., 2011; 2:211-232

TOPOLOGY OPTIMIZATION OF DOUBLE LAYER GRIDS FOR EARTHQUAKE LOADS USING A TWO-STAGE ESO-ACO METHOD

M. Mashayekhi, M.J. Fadaee, J. Salajegheh and E. Salajegheh[*, †]
Department of Civil Engineering, University of Kerman, Kerman, Iran

ABSTRACT

A two-stage optimization method is presented by employing the evolutionary structural optimization (ESO) and ant colony optimization (ACO), which is called ESO-ACO method. To implement ESO-ACO, size optimization is performed using ESO, first. Then, the outcomes of ESO are employed to enhance ACO. In optimization process, the weight of double layer grid is minimized under various constraints which artificial ground motion is used to calculate the structural responses. The presence or absence of elements in bottom and web grids and also cross-sectional areas are selected as design variables. The numerical results reveal the computational advantages and effectiveness of the proposed method.

Received: 10 February 2011; Accepted: 20 August 2011

KEY WORDS: double layer grids; topology optimization; earthquake loads; ant colony optimization; evolutionary structural optimization.

1. INTRODUCTION

Space structures belong to special category of three dimensional structures with special forms. These structures are widely used in exhibition centers, supermarkets, sport stadiums, etc., to cover large areas without intermediate columns. Space structures are often classified as grids, domes and barrel vaults [1]. Double layer grids are classical examples of prefabricated space structures and also the most popular forms which are used nowadays frequently.

Topology optimization methods enable designers to find a suitable structural configuration for required performances of structures [2]. Fuchs and Shemesh [3] used topology optimization to design of structures subjected to water pressure, Achtziger and Kocvara [4]

[*]Corresponding author: E. Salajegheh, Department of Civil Engineering, University of Kerman, Kerman, Iran
[†]E-mail address: eysasala@mail.uk.ac.ir

applied it on the maximization of the fundamental eigenvalue, and Maute and Allen [5] used it for design of aeroelastic structures.

The ground structure method is based on formulations of structural elements derived from fundamental mechanics. So, design engineers can easily understand the reasons for optimality and the mechanical viewpoints of the structure. Therefore, this type of optimization can offer important decision making support for structural engineers working at the conceptual design stage.

The ant colony optimization (ACO) is a relatively recent heuristic method to solve optimization problems simulating the behavior of real ant colonies. ACO similar to genetic algorithm is a good choice for structural topology optimization due to their discrete characteristics [6]. In topology optimization, the operation of these heuristic methods can be increased by combining with gradient-based methods. For example, in [7] a two-stage optimization method has been introduced for reliability-based topology optimization (RBTO) of double layer grids which has been performed by employing the methods of moving asymptotes (MMA) and ACO. Also in [7], the presence or absence of nodes (joints) in bottom grid and also cross-sectional areas have been selected as design variables.

Large scale double layer grids are subjected to vertical earthquake loads. Therefore, there is a great need for optimization methods which use these loads to calculate the structural responses [8].

In this paper, a new combined method for topology optimization of double layer grids is presented that considers vertical earthquake loading. The optimization is performed using the evolutionary structural optimization (ESO) and ant colony optimization (ACO) method, which is called ESO-ACO method. To execute ESO-ACO, a size optimization is performed using ESO in which the nonzero optimum cross-sectional areas are calculated from continuous quantities, first. Then, the obtained optimum cross-sectional areas and the internal forces of members (elements) are employed in ACO to improve the ACO approach as: (I) finding the structural importance rate of elements and using this to assign an unequal amount of pheromone on the paths that associates with the presence or absence of the members variable, (II) limiting the lower border of available cross-sectional areas of each element group to the neighborhood of the obtained cross-sectional areas by ESO, (III) determining the number of compressive and tensile element types and (IV) modifying the generation of random stable structures.

Through numerical examples, the optimum topologies of a double layer grid which obtained by ESO-ACO and ACO, are compared. The numerical results reveal the robustness and performance of ESO-ACO for topology optimization of skeletal structures with discrete cross-sectional areas and various constraints.

2. TOPOLOGY OPTIMIZATION WITH TIME HISTORY LOADING

In double layer grids topology optimization, geometry of the structure, support positions and coordinates of nodes are kept constant while the presence or absence of elements in bottom and web grids and also cross-sectional areas are selected as design variables. The symmetry properties of the structure are used for the tabulation of elements, which leads to decrease the

design space. Therefore, the elements are deleted in groups of 8 or 4 elements. For example in the structure shown in Figure 1, number of elements with similar geometry positions is arranged in Table 1.

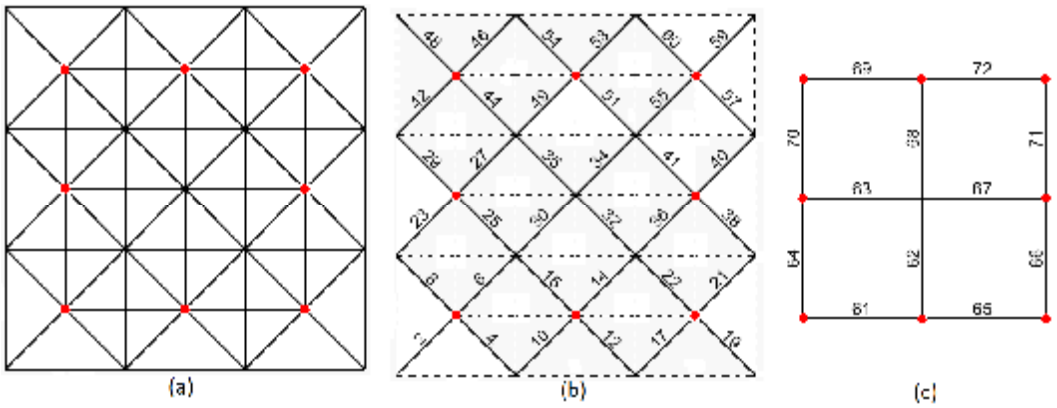

Figure 1. Double layer grid ground structure (a), element numbers of web layer (b) and element numbers of bottom layer (c)

Table 1. Elements group considering symmetry

Group Number	Elements in each group
1	61, 64, 70, 69, 72, 71, 66, 65
2	62, 63, 68, 67
3	2, 48, 59, 19
4	4, 8, 42, 46, 60, 57, 17, 21
5	23, 29, 54, 53, 38, 40, 10, 12
6	6, 44, 55, 22
7	25, 15, 27, 49, 51, 41, 14, 36
8	30, 35, 34, 32

Presence or absence of each element group is identified by a variable (topology variable), which only two digits 0 or 1 can be allocated to it. A zero amount of *i*th topology variable indicates that the *i*th element group should be deleted from the ground structure.

In topology optimization problem, the number of design variables (*NDV*) is the summation of the number of topology variables (*NTV*) and the type number of compressive and tensile members. For example during the topology optimization procedure of ground structure shown in Figure 1, the vector of design variables of a structure is identified as shown in Figure 2. In this Figure, it is assumed that the type number of compressive and tensile members is considered as 6 and 3, respectively.

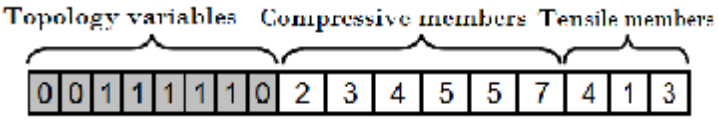

Figure 2. The identified design variables

Since the 1st, 2nd and the 8th topology variable have a zero value, all of the members in these groups of Table 1 are deleted from the ground structure. The result topology is shown in Figure 3.

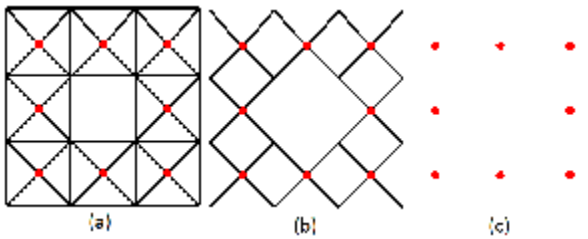

Figure 3. The result topology of Figure 2: (a) double layer grid, (b) diagonal layer, and (c) bottom layer

The remaining 9 design variables are used to assign the cross-sectional area to members in any group (type) by referring to the table of available profiles.

In order to achieve a practical structure, existence of members in top grid will not be considered as variable. This causes that the load bearing areas of top layer joints will not change. Also, discrete variables are used for optimizing the cross-sectional area of structural members. These variables are selected from pipe sections with specified thickness and outer diameter.

In optimum topology design of the double layer grids subjected to time history loading, the optimum amounts of design variables are found from discrete values to minimize the weight of the structure (W) under constraints on stress (g_σ), slenderness ratio (g_λ) and displacement (g_δ):

$$\begin{aligned} &Find: \ \overline{\mathbf{A}} = [J_1, J_2, ..., J_{NTV}, a_1, a_2, ..., a_{NMG}]^T \\ &J_i \in (0,1), \quad i = 1,2,...,NTV \\ &a_k \in \tilde{\mathbf{A}}, \quad k = 1,2,...,NMG \end{aligned} \tag{1}$$

$$\text{to minimize} : W(\overline{\mathbf{A}}) = \rho^e \sum_{k=1}^{NMG} a_k \sum_{i=1}^{N_k} l_i \tag{2}$$

$$subject\ to: \ g_{s,l,d}(\overline{\mathbf{A}}, \ddot{\mathbf{U}}(t), \dot{\mathbf{U}}(t), \mathbf{U}(t), t) \le 0, \ 0 \le t \le T \tag{3}$$

$$\mathbf{M}\ddot{\mathbf{U}}(t) + \mathbf{C}\dot{\mathbf{U}}(t) + \mathbf{K}\mathbf{U}(t) = -\mathbf{M}\mathbf{I}\ddot{\mathbf{U}}_g(t) \tag{4}$$

where N_k is the number of members in kth member group, a_k is the discrete cross-sectional area of the kth member group which selected from steel pipes in a given profile list ($\tilde{\mathbf{A}}$), ρ^e is

the material density, l_i is the length of the ith element, $\ddot{\mathbf{U}}_g(t)$ is ground acceleration at the time t, T is the time interval over which the constraints need to be applied, **M**, **C**, **K** and **I** are the mass, damping, stiffness and identity matrices; $\ddot{\mathbf{U}}_g(t)$, $\dot{\mathbf{U}}(t)$ and $\mathbf{U}(t)$ are the acceleration, velocity and displacement vectors of structure, respectively.

In time-dependent optimization problems, the stress and the slenderness ratio constraints are taken as:

$$g_s(\overline{\mathbf{A}},t)=\sum\nolimits_k \max\left(\left|s_k(\overline{\mathbf{A}},t)\right|\Big/\overline{s}_k(t)-1,\,0\right) \tag{5}$$

$$g_l(\overline{\mathbf{A}})=\sum\nolimits_k \max\left(l_k(\overline{\mathbf{A}})\Big/\overline{l}_k-1,\,0\right) \tag{6}$$

where s_k, $\overline{s}_k$, l_k and $\overline{l}_k$ are the member stress, allowable stress, member slenderness ratio and its upper limit for the kth member of double layer grids, respectively. In this study, the AISC code provisions are employed for the stress limits and local buckling criteria [9], as follows:

$$\begin{aligned}&\overline{s_k}(t)=0.6F_y \quad \text{(for tension members at the time t)}\\ &\overline{\sigma_k}(t)=\overline{\sigma_c} \quad \text{(for compression members at the time t)}\end{aligned} \tag{7}$$

in which

$$\overline{s_c}=\begin{cases}\left[\left(1-\dfrac{l_k^2}{2C_c^2}\right)F_y\right]\Big/\left(\dfrac{5}{3}+\dfrac{3l_k}{8C_c}-\dfrac{l_k^3}{8C_c^3}\right) & \text{for } l_k<C_c\\ \dfrac{12p^2E}{23l_k^2} & \text{for } l_k\geq C_c\end{cases} \tag{8}$$

where F_y is the yield stress, E is the modulus of elasticity and C_c is taken as $\sqrt{2p^2E/F_y}$.

The maximum slenderness ratio is limited to 300 and 240 for tension and compression members, respectively. Hence, the slenderness related design constraints can be formulated as follows:

$$\begin{aligned}&l_k=K_kl_k/r_k\leq\overline{l}_k=300 \quad \text{(for tension members at the time t)}\\ &\lambda_k=K_kl_k/r_k\leq\overline{l}_k=240 \quad \text{(for compression members at the time t)}\end{aligned} \tag{9}$$

where K_k is the effective length factor of the kth member (K_k=1 for all truss members) and r_k is its radii of gyration.

In time-dependent optimization process, the allowable vertical displacement (δ_V) is adopted as the width of double layer grids/360 [10]. The displacement constraint is expressed as follows:

$$g_d(\overline{\mathbf{A}},t)=\sum\nolimits_j \max\left(\left|d_j(\overline{\mathbf{A}},t)\right|\Big/d_V-1,\,0\right) \tag{10}$$

where δ_j is the displacement of the jth node.

To compute the response of structures subjected to time history loading, time history

analysis should be implemented. All of the time-dependent stress and displacement constraints need to be applied at each point in the desired time interval. To achieve this aim, the time interval is divided into n_{tp} subintervals and the time-dependent constraints are imposed at each time grid point. Because the total time interval is divided into n_{tp} subintervals, the constraint (3) is replaced by the constraints at the n_{tp}+1 time grid points as [11]:

$$g_{s,l,d}(\bar{\mathbf{A}}, \ddot{\mathbf{U}}(t_j), \dot{\mathbf{U}}(t_j), \mathbf{U}(t_j), t_j) \le 0, \ j = 0,1,...,n_{tp} \tag{11}$$

For analysis of the structures subjected to earthquake loading, software framework OpenSees [12] is used. The OpenSees is an open source object-oriented software framework for static and dynamic, linear and nonlinear finite element analysis of structural systems. In this study, the step by step time integration algorithm of Newmark [13] is used in conjunction.

To solve a constrained optimization problem, its objective function (W) should be modified in such a way that the constrained problem should be converted to an unconstrained one. Thus only one modified objective function (Ψ) is minimized [11]. In this paper, Ψ is defined as:

$$\Psi(\bar{\mathbf{A}}) = W(\bar{\mathbf{A}})(1 + C(\bar{\mathbf{A}}))^2 \tag{12}$$

in which

$$C(\bar{\mathbf{A}}) = \sum_{j=0}^{n_{tp}} \left[\sum_{i=1}^{ne} (g_{s,i}(\bar{\mathbf{A}}, t_j) + g_{l,i}(\bar{\mathbf{A}}, t_j)) + \sum_{j=1}^{nj} g_{d,j}(\bar{\mathbf{A}}, t_j) \right] \tag{13}$$

where C is the penalty function, ne is the number of elements and nj is the number of joints.

The optimum topology design of double layer grids is a minimization problem, and hence the fitness function must be chosen such that the higher the weight of a structure, the lower is its fitness and vice-versa. The following relation is selected as the measure of fitness function [14]:

$$F_i = \Psi_{\max} + \Psi_{\min} - \Psi_i \tag{14}$$

where $\Psi_{\max}$, $\Psi_{\min}$ and Ψ_i are the maximum and minimum modified objective function value in a cycle and the modified objective function value of the ith structure, respectively.

As two methods ACO and ESO are combined, in order to make the paper self-descriptive, first the features of ACO and ESO are briefly explained in Sections 3 and 4, respectively. Then the characteristics of ESO-ACO are described in Section 5.

3. ANT COLONY OPTIMIZATION (ACO)

ACO method is an algorithm that tries to simulate the real social behavior of ant colonies. From nest to the food source, an ant deposits some quantity of pheromone on its path. Other ants tend to follow the paths probabilistically where the pheromone concentration is higher, adding themselves some quantity of pheromone. The aim of this process is to find the shortest (optimal) path. Also, pheromone is subjected to evaporation to increase the probability of

achieving the global optimal paths [15].

Camp and Bichon [16] employed the ACO method to find the optimum cross-sectional area for the elements of space trusses. In this study, their ACO methodology is used to find the optimum topology of double layer grids and cross-sectional area of elements.

The following step-by-step review shows the process of optimization.

Step 1: Set parameters, initial pheromone intensity τ_{ij} and amount of visibility η_{ij} associated with the path connecting variable *i* to variable *j*, as follows:

$$t_{ij} = t_0 = 1/[W_{\min}(1-r)], \begin{cases} 1 \le i \le NTV \Leftrightarrow 1 \le j \le 2 \\ NTV+1 \le i \le NDV \Leftrightarrow 1 \le j \le NP \end{cases} \tag{15}$$

$$\begin{aligned} h_{ij} &= 1, && 1 \le i \le NTV, 1 \le j \le 2 \\ h_{ij} &= 1/a_j, && NTV+1 \le i \le NDV, 1 \le j \le NP \end{aligned} \tag{16}$$

where $W_{\min}$ is the weight of structure resulting from assigning the smallest available profile to each member of the structure, (1-ρ) is the evaporation rate, *NP* is the number of available profiles and a_j is the cross-sectional area of the *j*th available profile.

Step 2: Combine visibility and trail (pheromone) concentration to obtain the ant decision table *D*, at the cycle t_c:

$$D_{ij}(t_c) = [t_{ij}(t_c)]^a [h_{ij}]^b \Big/ \sum_{l \in allowed} [t_{il}(t_c)]^a [h_{il}]^b \tag{17}$$

where *allowed* is set of neighboring variables from variable *i*, and α and β are constants.

Step 3: Compute $p_{ij}(t_c)$ that represents the probability to choose the *j*th quantity for the *i*th variable (0 or 1, for *i*th topology variable or an area for (*i-NTV*)th member group) at t_cth cycle as:

$$p_{ij}(t_c) = D_{ij}(t_c) \Big/ \sum_{l \in allowed} D_{il}(t_c) \tag{18}$$

Step 4: Decrease τ_{ij}, when the ant chooses the *j*th area for its (*i-NTV*) member group using (18), as follows (this pheromone lowering is not carried out for topology variables):

$$t_{ij}(t_c) = q.t_{ij}(t_c), 0 < q < 1, \begin{cases} NTV+1 \le i \le NDV \\ 1 \le j \le NP \end{cases} \tag{19}$$

Step 5: Repeat Steps 2 to 4 until all of the ants allocate an amount to primary variable, and the first iteration is completed.

Step 6: Repeat Steps 2 to 5 until each ant in colony has assigned an amount for its variables.

Step 7: Analyze all of the structures and update the trail intensity on the paths with respect to the structures fitness, as follows [17]:

$$t_{ij}(t_c+1)=(1-r)t_{ij}(t_c)+r\,(l\Delta t_{ij}^{+}(t_c)+\Delta t_{ij}^{r}(t_c)) \tag{20}$$

in which

$$\begin{aligned}\Delta t_{ij}^{+}(t_c)&=1/\Psi^{+}(t_c)\\ \Delta t_{ij}^{m}(t_c)&=(g-m)/\Psi^{m}(t_c)\\ \Delta t_{ij}^{r}(t_c)&=\sum_{m=1}^{g-1}\Delta t_{ij}^{m}(t_c)\end{aligned} \tag{21}$$

where $\Psi^{+}(t_c)$ is the modified objective function of the best solution from beginning of the cycle t_c, γ is the number of top ranked ants, μ is the rank of ant (between 1 and γ) and Ψ^{μ} is the modified objective function of the ant (structure) receiving rank μ.

Step 8: Terminate the optimization if a stopping criterion is satisfied. If not, return to Step 2.

In this paper, two convergence criteria are determined: (a) the best solution of each cycle remains fixed for 10 cycles, and (b) the number of cycles reaches to 100. After satisfying one of the convergence criteria, Phase 1 of the ACO search is completed (Figure 4) where in this figure *nAnt* and |**K** are the number of ants and the determinant of the stiffness matrix, respectively.

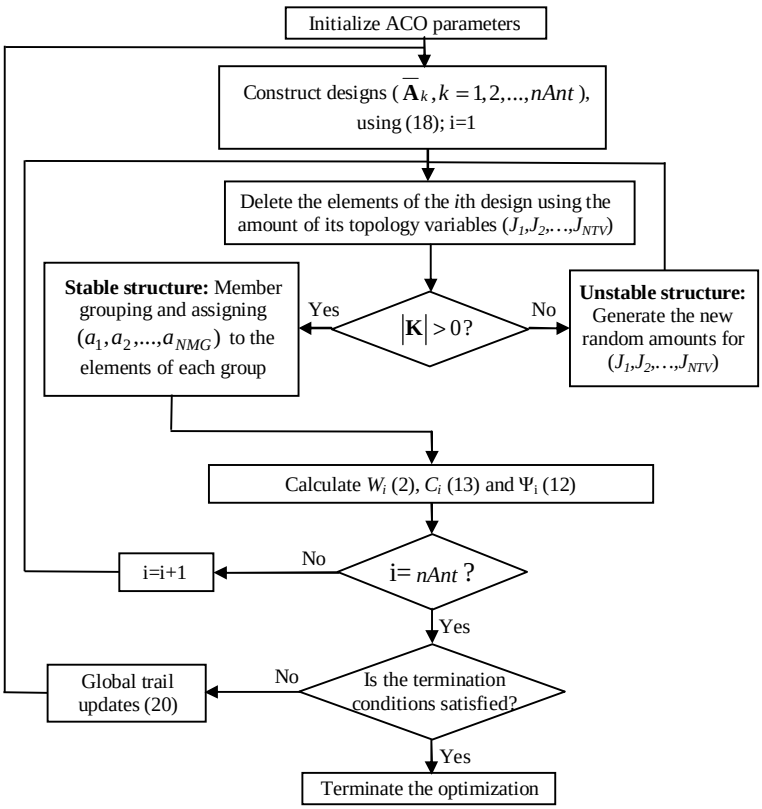

Figure 4. The flow chart for topology optimization using ACO

To motivate the ant colony to search for an improved solution, a Phase 2 local search is started by Camp and Bichon [16]. In this article, to achieve a better solution, at the end of this phase the local search space of the following phases is defined by the neighborhood of the

previous elitist ant's solution. The value of trail in each phase is reset to τ_0 for paths in the local search space and set to zero for all other paths. The size of each phase search space around the previous elitist ant is approximately evaluated 20% of its original size of available profile. The optimization in several phases is implemented until the optimum weight of the structure is not changed significantly in two successive phases.

4. EVOLUTIONARY STRUCTURAL OPTIMIZATION (ESO)

In this paper, in order to achieve better topology using ACO, some of the ACO parameters are improved so that in topology optimization the absence probability of important elements decreases. To achieve this aim, the size optimization is performed using ESO, first. Then, the location of members with high structural importance is identified using the optimum cross-sectional areas and the internal forces of members.

For size optimization of a structure, the following optimization problem is solved using ESO:

$$\begin{aligned} &Minimize: W(\mathbf{a}) = \rho^e \sum_{k=1}^{ne} a_k l_k \\ &Subject\ to: \mathbf{K}(\mathbf{a})\mathbf{d} = \mathbf{F} \\ &\quad |s_i| = \tilde{s}_i, \quad i = 1,...,ne \\ &\quad \mathbf{a} \in \hat{\mathbf{A}} = \left\{ \mathbf{a} \in R^{ne} : a_{\min} \le a_i \le a_{\max}, i = 1,...,ne \right\} \end{aligned} \tag{22}$$

where a_{min}, a_{max}, $\tilde{s}_i$, R^{ne}, **F** and **d** are the allowable minimum and maximum cross-sectional areas, the target stress of the *i*th element, a given set of continuous values, the load and displacement vectors, respectively.

The following step-by-step summary shows the process of optimization of (22) using ESO algorithm [18]:

Step 1: Set parameters, initial design variables $\mathbf{a}^0$ and the iteration counter k=0.

Step 2: Compute the displacement vector $\mathbf{d}(\mathbf{a}^k)$ for the current design by carrying out a finite element analysis: $\mathbf{d}(\mathbf{a}^k)=\mathbf{K}(\mathbf{a}^k)^{-1}\mathbf{F}$.

Step 3: For the current design $\mathbf{a}^k$, calculate the member stresses $(s_i, i=1,...,ne)$.

Step 4: Compare stress of the *i*th member with its target value $(\tilde{s}_i)$.

Step 5: If absolute stress is above target, increase area by a small increment (Δa); or if absolute stress is below target then decrease area by a small increment.

Step 6: If area reached prescribed lower or upper bound (a_{min} or a_{max}) then freeze area.

Step 7: Check to see if previously frozen areas need unfrozen.

Step 8: Put k=k+1, and return to Step 2 unless a stopping criterion is satisfied.

In this paper, the convergence criterion is assumed that the weight of the structure does not change significantly in two successive iterations:

$$\frac{|W_k - W_{k-1}|}{W_k} \times 100 < e, \ W_0 = 0 \tag{23}$$

5. TWO-STAGE OPTIMIZATION METHOD (ESO-ACO)

In topology optimization of double layer grids, topology and cross-sectional area of elements are two different classes of variables (Figure 2). In this paper, the ACO is modified in which this method can find better amounts for each class of variables.

In topology optimization process (Figure 4), the elements are deleted in two different parts: (a) constructing solutions, and (b) generating the new random amounts for topology variables of unstable structures. To search better amounts for topology variables, a strategy is applied in each part of (a) and (b) which are described in sections 5.1 and 5.2, respectively. Using these strategies causes that the absence probability of important elements is reduced.

The type number of compressive and tensile members is determined in Section 5.3. Finally, the optimum cross-sectional areas are found in a reduced search space (Section 5.4).

To achieve this aim, the optimization problem in (22) is first solved using ESO. Then, the obtained optimum cross-sectional areas and the internal forces of members are used to accomplish the following four modifications (Sections 5.1-5.4). With these adaptations, ACO effectively obtains the optimum topology that all of the stress, displacement and slenderness ratio constraints are satisfied and the cross-sectional areas are selected from discrete quantities i.e. Eqs. (1-4).

5.1 Determining the pheromones of the topology variables

In order to achieve a better topology, the importance rate of the *i*th group elements (IR_i) is calculated as follows:

$$IR_i = MA_i / MA_{\max}, MA_{\max} = \max(MA_i),\ i = 1,\ldots,nbwe \tag{24}$$

where MA_i is the cross-sectional area of a member of the *i*th group and *nbwe* is the number of bottom and web grids elements.

Thereafter, the pheromones of the presence or absence of the elements in *i*th group is identified as follows:

$$\begin{aligned} \boldsymbol{\tau}(i,1) &= \max[\tau_{\min}, \tau_0(1-IR_i)] \\ \boldsymbol{\tau}(i,2) &= \max[\tau_{\min}, \tau_0(IR_i)] \end{aligned} \tag{25}$$

where $\boldsymbol{\tau}(i,1)$ and $\boldsymbol{\tau}(i,2)$ are the pheromone of the absence and presence of *i*th group elements, respectively. Therefore the more IR_i means more presence pheromone of the *i*th group elements and the existence probability of these elements in structure increases. τ_{min} is the minimum pheromone that the following formulations are adopted [19]:

$$\tau_{\min} = \tau_0(\tau_1/\tau_2) \tag{26}$$

where

$$\tau_1 = (1\text{-}0.05^{(1/NDV)})$$
$$\tau_2 = [(-1 + NDV/2) \times 0.05^{(1/NDV)}] \quad (27)$$

5.2 Enhancing the generation of new random stable structures

Numerous unstable structures are produced in topology optimization procedure of double layer grids using ACO and ESO-ACO. In this article, after finding each unstable structure, a new random structure is constructed and then its stability is checked. This process is continued until a stable structure is produced. To increase the efficiency of ESO-ACO for producing a new structure, *i*th group elements are deleted randomly from the ground structure if the following relationship is satisfied:

$$IR_i \le IR_{\min} \quad (28)$$

where IR_{min} is the minimum importance rate. Selecting a small amount of IR_{min} removes a few numbers of elements. Also, if IR_{min} is selected a large amount, near to one, large number of elements are subjected to delete randomly. It causes that removing chance of elements which have large and small amount of *IR*, will be equal. So the amount of IR_{min} should be chosen such that the proper number of elements will be deleted by chance.

5.3 Identifying the type number of compressive and tensile members

After solving the optimization problem (22), the member forces are found. With consideration of the stress and slenderness ratio constraints in design stage, the proper cross-sectional area is chosen from available profiles for any member with tensile and compressive internal force to satisfy the mentioned constraints.

After designing all of the members, the members that have the same cross-sectional area are located in the same type, with respect to compressive and tensile internal force. Then, counting the various cross-sectional areas determines the number of compressive and tensile element types.

5.4 Lowering the available list profile for elements of each type

The allocated profile to each element in Section 5.3 is based on the optimization problem (22) which has only two constraints. When in the optimization problem, there are several constraints such as stress, displacement and slenderness ratio, subject to static and dynamic loads, greater cross-sectional area should be probably assigned to the elements. Therefore the allocated cross-sectional area to the elements in Section 5.3 can be considered approximately as the lowest limit of the available profile. To have more security, the following relationship is suggested to the lowest limit of available profile for *i*th elements type (lb_i):

$$lb_i = dp_i - 0.1(NP),\ lb_i \ge 1 \quad (29)$$

where dp_i is the digit of the assigned profile for *i*th elements type which is calculated in Section 5.3.

The process of ESO-ACO method is schematically shown in Figure 5.

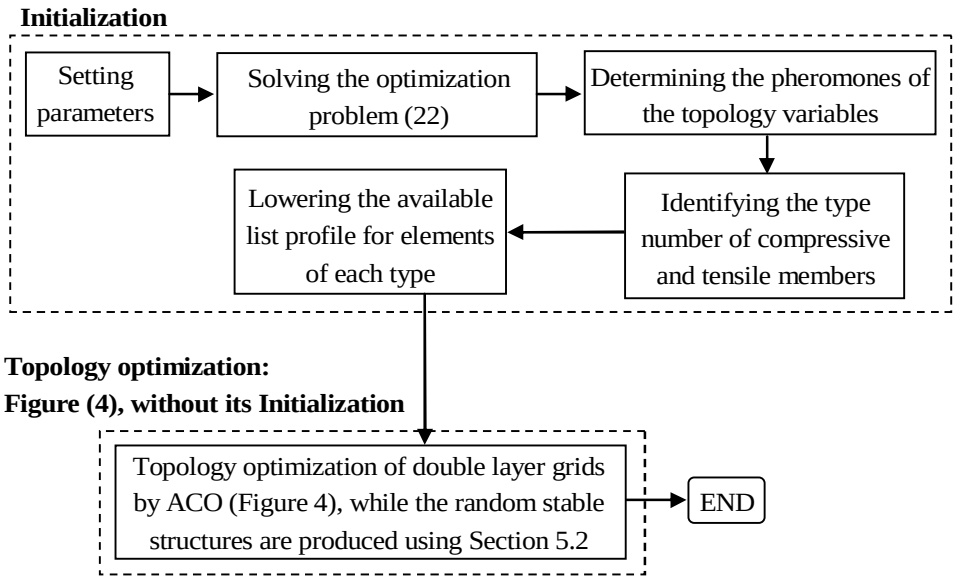

Figure 5. The flowchart of ESO-ACO method

6. ARTIFICIAL EARTHQUAKES

For seismic design of structures, either response spectrum or dynamic time history analysis subjected to earthquake is required. The dynamic time history analysis has shown its superiority both in accuracy and efficiency as compared to other methods [20]. It is then necessary to have accelerograms that has compatible characteristics and seismic excitation with desired site. Therefore, it is often difficult or may be impossible in some cases to choose a proper record for a site, because historically recorded accelerograms for the given site are scare. Hence, artificial earthquakes that are statistically influenced by desired properties of the given site are very useful for seismic design of structures. A number of approaches based on time domain and frequency domain have been proposed for the generation of synthetic ground motion records. In this paper, spectral representation method based on time domain procedure is used. The non-stationary ground motion $(\bar{a}(t))$ is simulated using this method as [21]:

$$\bar{a}(t) = I_m(t) \sum_{n=1}^{NFR} \{4 S_{KT}(n\Delta f)[1+d_S R_N]\Delta f\}^{1/2} \sin(2p\, n\Delta f\, t + q_n) \qquad (30)$$

where $I_m(t)$ and $S_{KT}(.)$ are the modulation function and the specific power spectral density function (PSDF), respectively. NFR is the number of sine functions or frequencies included, between 0 and $f_{\max}$, d_S and R_N are the coefficient of variation and a standard normal variable that used in ordinates of PSDF, Δf is frequency step, and q_n are random phase angles with a uniform distribution between 0 and $2p$. In this study, the modulation function expressed in

[22] is used as follows:

$$I_m(t)=\begin{cases}(t/T_1)^d & 0\le t\le T_1\\ 1 & T_1\le t\le T_2\\ e^{-c(t-T_2)} & T_2\le t\le T\end{cases} \tag{31}$$

where T_1, T_2 and T are specific times and the duration of the simulated record, d and c are constants. Also, the PSDF of the non-stationary ground motion suggested by Clough and Penzien [13] is considered as:

$$S_{KT}(f)=S_0\left[\frac{1+4x_g^2(\frac{f}{f_g})^2}{(1-(\frac{f}{f_g})^2)^2+4x_g^2(\frac{f}{f_g})^2}\right]\left[\frac{(\frac{f}{f_g})^4}{(1-(\frac{f}{f_g})^2)^2+4x_f^2(\frac{f}{f_g})^2}\right] \tag{32}$$

where S_0 is the constant PSDF of input white-noise random process; f_g and x_g are the characteristic ground frequency and the ground damping ratio; f_f and x_f are parameters for a high-pass filter to attenuate low frequency components. The parameters for the generation of simulated ground motion are selected according to values that proposed by Moller *et al.* [23] as following:

Table 2. The parameters for generation of simulated ground motion

Parameter	$a_G \le 350\,cm/s^2$	$350 \le a_G \le 700\,cm/s^2$	$a_G \ge 700\,cm/s^2$
T (sec)	5.12	10.24	20.48
T_1 (sec)	0.50	1.50	2.00
T_2 (sec)	4.00	8.00	16.00
c	2.0	1.0	0.7
d	2.0	2.0	2.0
NFR	100	200	300
f_{max} (Hz)	12	15	15
d_S	0.40	0.40	0.40

Numerical integration of artificial ground motions in the time domain often results in non-physical shifts in velocity and displacement time histories. Many methods are available to perform correction of artificial ground motion and eliminate the unrealistic velocity or displacement drift. In this paper, the method proposed by Yang *et al.* [24] is used for this purpose. In this approach, the baseline correction is firstly imposed on the data of artificial

ground motion in the time domain using the least-square curve fitting technique, and then a windowed filter in the frequency domain is used to eliminate the components that cause long-period oscillations in the derived displacement. The corrected record is finally compatible with the code design spectrum and is scaled to a peak acceleration a_G, a random peak value that could occur at the site in case of an earthquake.

Because of the time consuming analysis of double layer grids subjected to earthquake loading, in this paper T is selected as the smallest value of Table 2 (5.12 sec). Also, a_G is assumed as 0.3 times the gravity acceleration (294 cm/s^2). Therefore, the parameters for generation of ground motion are selected from the first column of Table 2. The modified simulated ground motion is shown in Figure 6.

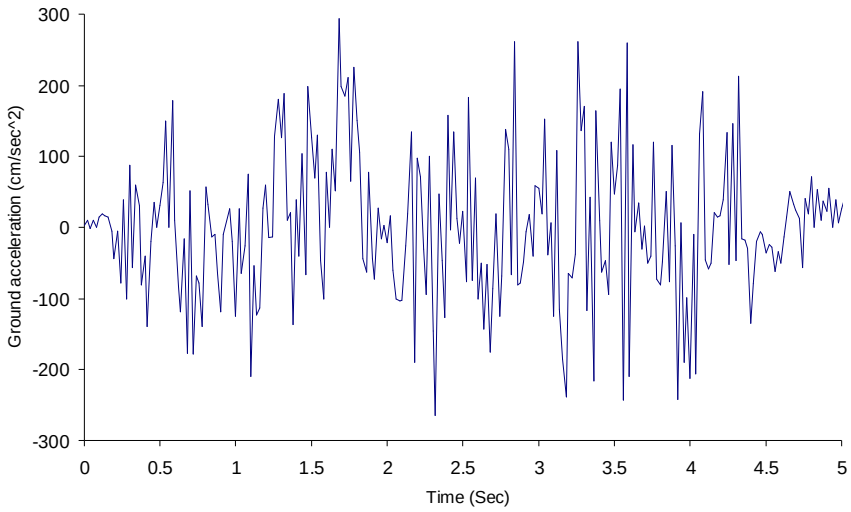

Figure 6. The modified obtained artificial ground motion

These types of artificial records have been used in literature as horizontal ground acceleration. According to code of practice for skeletal steel space structures [25], the ratio of response spectrum values of the vertical earthquake to horizontal one must be selected more than 0.667. Also, it is recommended that for the space structures with periods more than 0.2 sec, this minimum ratio to use. It is noted that in focal or near fault regions, this minimum ratio is registered more than 1 for periods that are less than 0.1 sec [25]. In this paper, for more safety, this minimum ratio is considered as 1 instead of 0.667. Therefore, the artificial ground motion shown in Figure 6 is selected as vertical ground acceleration.

7. EXAMPLE: 10×10 DOUBLE LAYER GRID

A square-on-square double layer grid with 221 nodes and 800 elements is presented to examine and verify the proposed optimization method. The depth of the double layer grid and the node spacing in the top and bottom chord is 290 cm and 400 cm, respectively. The ground structure is assumed to be supported at perimeter nodes of bottom grid (Figure 7).

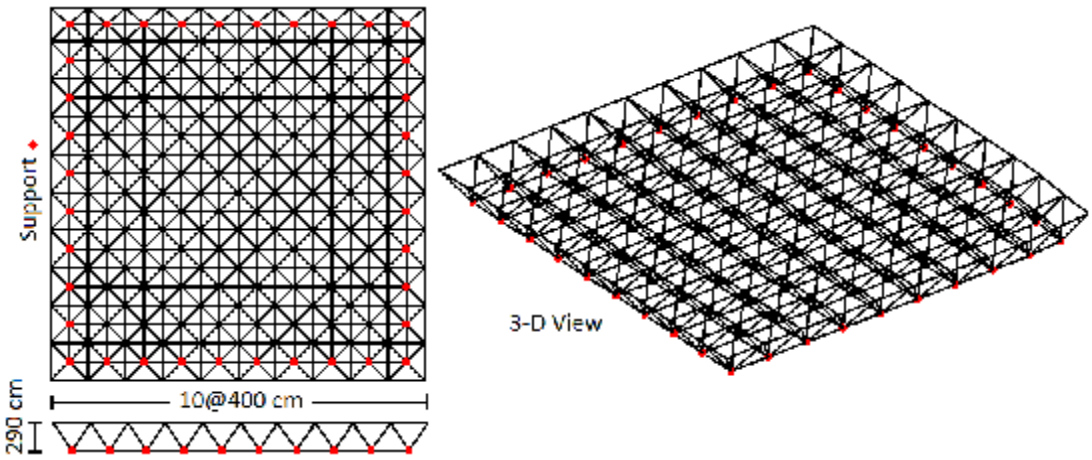

Figure 7. A 10×10 double layer grid

The assumed material is steel with a Young's modulus and mass density of 2.1×10^6 kg/cm^2 and 7850 kg/m^3, respectively. Gravity acceleration is considered as 981 cm/s^2 and the dead load (*DL*) on double layer grid is 180 kg/m^2. This distributed load is assigned to the nodes of the top grid in the proportion of their load bearing area [26].

The cross-sectional area of members is selected from the pipe profiles available in Table 3, where *OD* and *TH* are outer diameter and thickness in centimeter, respectively.

Table 3. Available pipe profiles

No.	***OD***	***TH***	**No.**	***OD***	***TH***	**No.**	***OD***	***TH***	**No.**	***OD***	***TH***
1	4.83	0.26	6	10.80	0.36	11	16.86	0.45	16	32.39	0.71
2	6.03	0.29	7	11.43	0.36	12	19.37	0.45	17	35.56	0.80
3	7.61	0.29	8	13.30	0.40	13	21.91	0.45	18	40.64	0.88
4	8.89	0.32	9	13.97	0.40	14	24.45	0.63	19	45.72	1.00
5	10.16	0.36	10	15.90	0.45	15	27.30	0.63			

The number of ant, γ, ρ and θ are selected as 100, 10, 0.5 and 0.67, respectively [16]. The computational results show that the other specifications of ACO and ESO-ACO which are shown in Table 4 are good choices.

Table 4. Specifications of ACO and ESO-ACO methods

Parameter	α	β	a_{min} (cm^2)	a_{max}(cm^2)	Δa(cm^2)	IR_{min}	e	$\tilde{s}_i$ (kg/cm^2)	
								Tension members	Compression members
Value	1	0.2	1.5	50	0.05	0.2	0.001	1440	1200

The bottom and diagonal members are tabulated in 80 different groups (*NTV*=80). Using the values of Table 4, the optimization problem (22) is solved, and the number of member types is obtained as 3 for tensile members and 12 for compressive members (Section 5.3), which resulted in 95 design variables. The optimum structure is shown in Figure 8, in which the thickness of each element is directly proportional to its cross-sectional area.

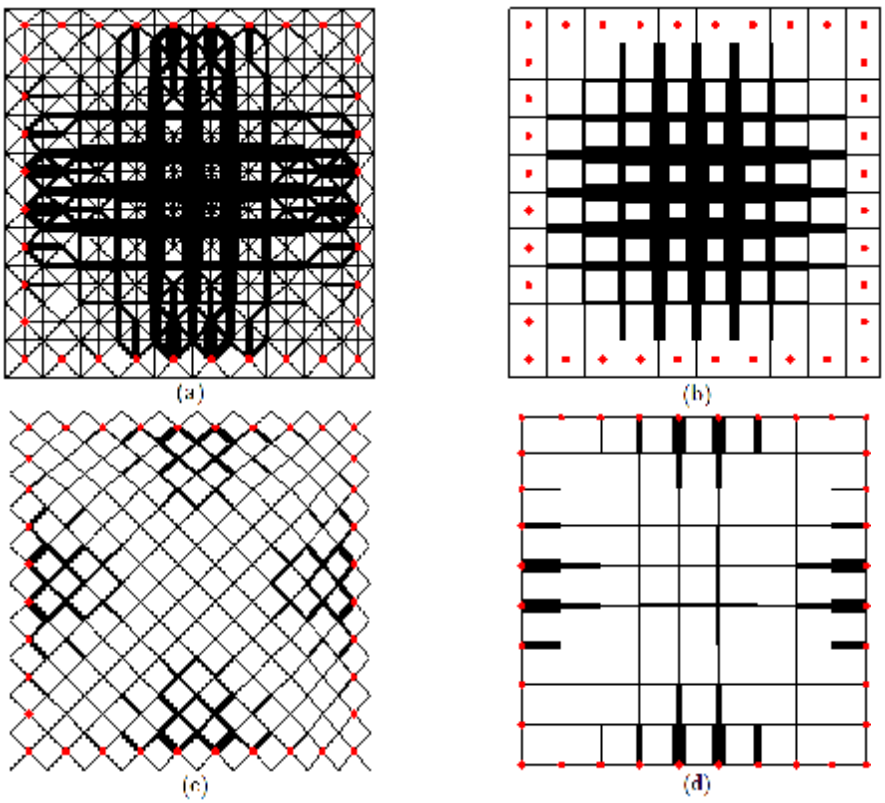

Figure. 8 The optimum structure using the ESO: (a) double layer grid, (b) top layer, (c) diagonal layer, and (d) bottom layer

Considering IR_{min}=0.2, stating in (28), causes that the positions of members which are allowable and unallowable to delete randomly, are determined as shown in Figure 9 with the same small and large thickness, respectively.

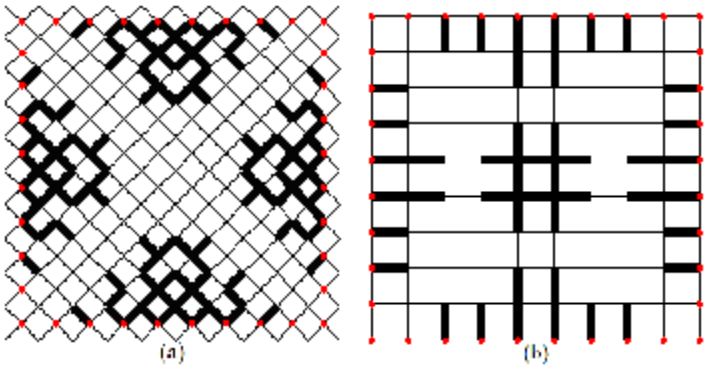

Figure. 9 The positions of members which are allowable and unallowable to delete randomly: (a) diagonal layer, (b) bottom layer

This example is optimized in three cases as follows:

Case 1: Size optimization of the ground structure.

Case 2: Topology optimization using ACO.

Case 3: Topology optimization using ESO-ACO.

In each of these three cases, the constraints should be calculated for load combinations proposed by AISC code. The load combinations are as follows [9]:

$$\begin{aligned} &Static\ Loading : DL \\ &Dynamic\ Loading : 0.75(DL \pm E_z) \end{aligned} \tag{33}$$

where E_Z is the vertical time history loading. Also, for dynamic loading, the constraints are checked at 257 grid points with time step of 0.02 sec.

The members are grouped for reduction of the search space. To achieve this aim, an introductory static analysis is first performed in which all members have the same cross-sectional area. Then, the entire range of axial forces is divided into several equal ranges for both of the tension and compression members. Each member of the double layer grid is placed into various groups according to its amount of axial force. It is noted that the number of these equal ranges for tension and compression members are determined in Section 5.3.

To consider the stochastic nature of the ACO and ESO-ACO approaches, seven sample optimization runs are performed for each design case and the achieved optimal solutions for Cases 1 to 3 are presented.

In all of the following figures, (a), (b), (c) and (d) are double layer grid, top layer, diagonal layer and bottom layer, respectively. Furthermore in these figures the thickness of each element is directly proportional to its cross-sectional area.

7.1. Static Loading

In Cases 1, 2 and 3, the optimum structures are shown in Figures (10-12), which the optimum weights of these structures are obtained as 21497 kg, 17256 kg and 15979 kg, respectively.

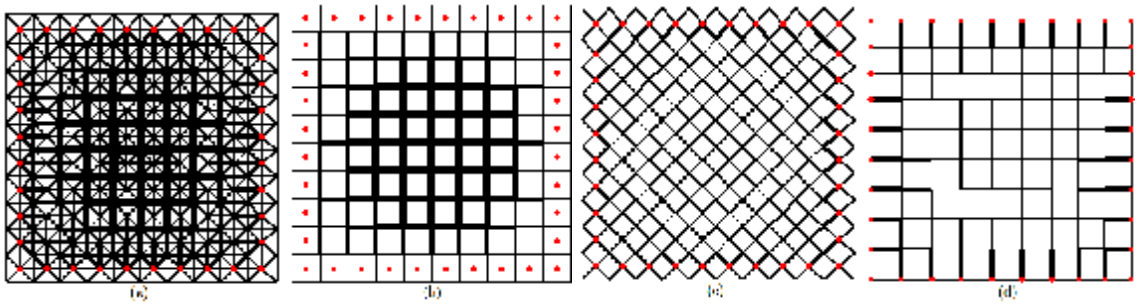

Figure 10. Optimum ground structure in Case 1

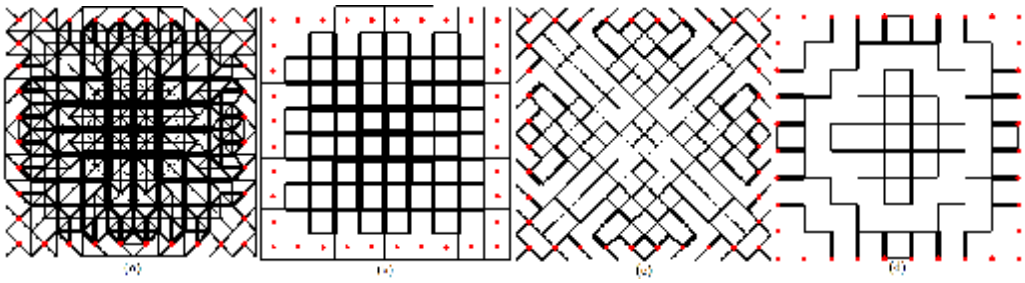

Figure 11. Optimum topology in Case 2

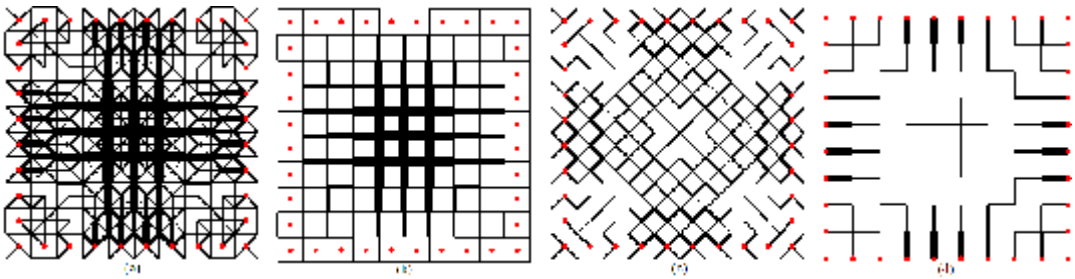

Figure 12. Optimum topology in Case 3

7.2. Dynamic Loading

The optimum structures in Cases 1, 2 and 3, are shown in Figures (13-15), where the optimum weights of these structures are obtained as 22880 kg, 19581 kg and 18285 kg, respectively.

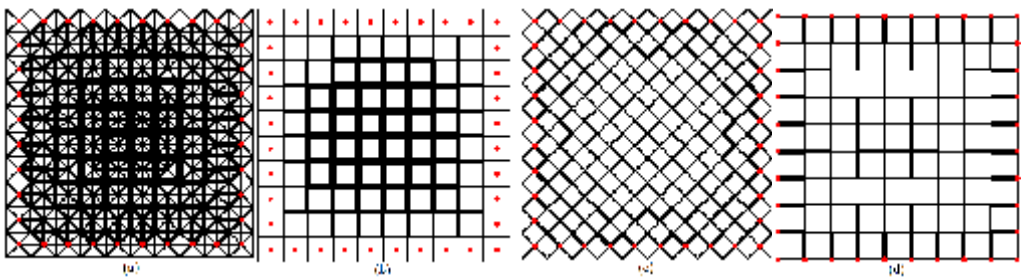

Figure 13. Optimum ground structure in Case 1

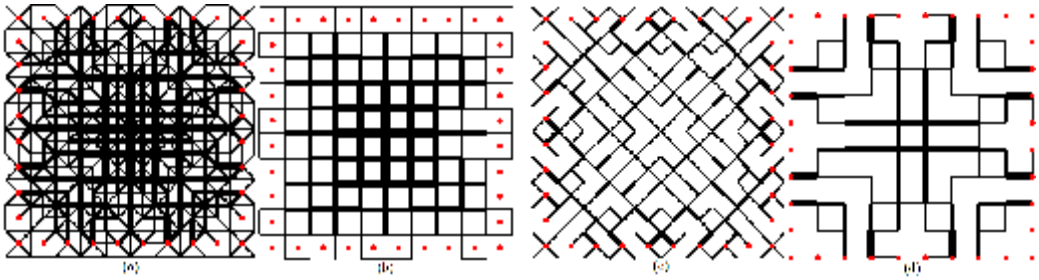

Figure 14. Optimum topology in Case 2

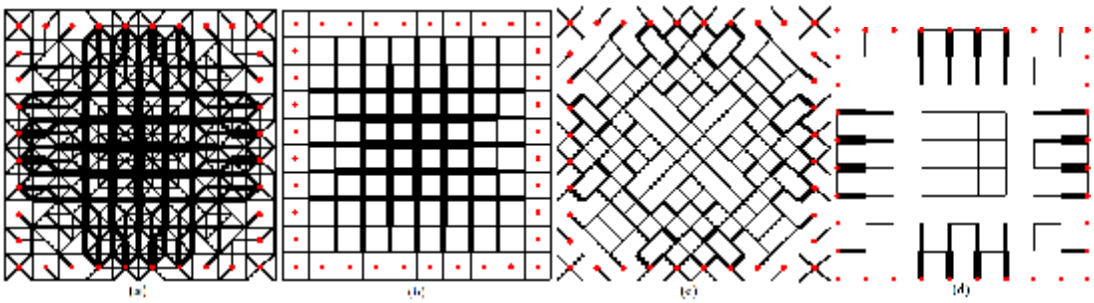

Figure 15. Optimum topology in Case 3

The best optimum weights of all cases are listed in Table 5 to compare with each other.

Table 5. Comparison of the optimum weights of structure for Cases 1, 2 and 3

Loading	**Optimum Weight (kg)**		
	Case 1	**Case 2**	**Case 3**
Static	21497	17256	15979
Dynamic	22880	19581	18285

These values validate that topology optimization of double layer grids achieves better weight than their size optimization with the same constraints.

To evaluate the better comparison of ACO and ESO-ACO to achieve the optimum topologies, optimum weights of the topologies attained for Cases 2 and 3 are listed in Table 6 for seven sample runs where the weight of topologies shown in Figures. (11, 12, 14 and 15) is highlighted.

Table 6. Optimum weights of the topologies attained for Cases 2 and 3 for seven sample runs

Loading	Case No.	Optimum Weight (kg)						
		Sample 1	Sample 2	Sample 3	Sample 4	Sample 5	Sample 6	Sample 7
Static	2	17913	18526	17583	17256	17340	17522	17418
	3	16745	17186	17288	16616	15979	16487	16756
Dynamic	2	22895	20365	20844	20144	21879	19581	21842
	3	18778	19437	18285	19676	19830	18832	18733

The mean ($\overline{W}$) and the standard deviation (*SD*) of these optimum weights with *ns* testing samples are listed in Table 7 and are calculated as follows:

$$\overline{W} = \frac{\sum_{i=1}^{ns} W_i}{ns} \tag{34}$$

$$SD = \sqrt{\frac{\sum_{i=1}^{ns} (W_i - \overline{W})^2}{ns - 1}} \tag{35}$$

Table 7. The mean and the standard deviation of the optimum weights

Loading	Case No.	$\overline{W}$ (kg)	*SD* (kg)
Static Loading	2	17651	440
	3	16722	439
Dynamic Loading	2	21079	1169
	3	19082	570

All of the statistical values of Table 7 demonstrate that the ESO-ACO in topology optimization of double layer grids achieves better performance than the ACO with consideration of various loadings. It is noted that although for static loading the *SD* of Cases 2 and 3 are approximately the same, but observing Table 7 indicates that in six samples, Case 3 achieves lower weight than the smallest weight in Case 2.

8. CONCLUSIONS

In this paper, a two-stage optimization method (ESO-ACO) has been proposed for topology optimization of double layer grids subject to static and time-history loading (e.g. earthquake)

and uses ground structure approach. In optimization process of ESO-ACO, the weight of the structure is minimized under constraints on stress, slenderness ratio and displacement which artificial ground motion is used to calculate these structural responses.

For implementation of ESO-ACO, the location of members with high structural significance was first recognized. To achieve this aim, the solution of the size optimization problem was found using ESO. Then the outcomes of ESO (optimum cross-sectional areas and the internal forces of members) were used to improve ACO through four modifications.

The proposed method was applied for topology optimization of a double layer grid and the optimization was implemented in three cases which their results are as follows: (a) ESO-ACO method obtains the optimum topologies with lower weight than those of optimum topologies attained by ACO with consideration of various constraints, (b) ESO-ACO approach is more reliable than ACO. With respect to the ACO method, ESO-ACO has better solutions and standard deviations, and (c) topology optimization of double layer grids causes that these structures satisfy the various constraints, subject to static and dynamic loads, with better weight than that of the size optimization of ground structures.

REFERENCES

1. Parke G, Disney P. *Space Structures 5*, Thomas Telford, London, 2002.
2. Bendsøe MP, Sigmund O. Topology Optimization: Theory, Methods and Applications, Springer, Berlin, 2004.
3. Fuchs MB, Shemesh NNY. Density-based topology design of structures subjected to water pressure using a parametric loading surface, *Struct Multidiscip Optim* 2004; **28**: 11-9.
4. Achtziger W, Kocvara M. On the maximization of the fundamental eigenvalue in topology optimization, *Struct Multidiscip Optim* 2007; **34**: 181-95.
5. Maute K, Allen M. Conceptual design of aeroelastic structures by topology optimization structures, *Struct Multidiscip Optim* 2004; **27**: 27-42.
6. Kaveh A, Hassani B, Shojaee S, Tavakkoli SM. Structural topology optimization using ant colony methodology, *Eng Struct* 2008; **9**(30): 2559– 65.
7. Mashayekhi M, Salajegheh E, Salajegheh J, Fadaee MJ. Reliability-based topology optimization of double layer grids using a two-stage optimization method, *Struct Multidiscip Optim* (SMO-10-0245, under review).
8. Gholizadeh S, Salajegheh E. Optimal design of structures subjected to time history loading by swarm intelligence and an advanced metamodel, *Comp Meth Appl Mech Eng* 2009; **198**: 2936-49.
9. American Institute of Steel Construction, AISC Manual, 2005.
10. Salajegheh E, Mashayekhi M, Khatibinia M, Kaykha M. Optimum shape design of space structures by genetic algorithm, *Int J Space Structures* 2009; **24**(1): 45-58.
11. Kang BS, Park GJ, Arora JS. A review of optimization of structures subjected to transient loads, *Struct Multidiscip Optim* 2006; **31**: 81-95.
12. Open Sees, *Open System for Earthquake Engineering Simulation*, Pacific earthquake engineering research centre, University of California, Berkeley, (Release 2.2.2), 2010, http://opensees.berkeley.edu/.

13. Clough RW, Penzien J. *Dynamics of Structures*, Mc Graw Hill, New York, 1975.
14. Krishnamoorthy CS, Prasanna VP, Sudarshan R. Object-oriented framework for genetic algorithm with application to space truss optimization, *J Comput Civ Eng* 2002; **16**(1): 66-75.
15. Dorigo M, Stützle T. *Ant Colony Optimization*, A Bradford Book, Massachusetts Institute of Technology, USA, 2004.
16. Camp CV, Bichon BJ. Design of space trusses using ant colony optimization, *J Struct Eng, ASCE* 2004; **130**(5): 741-51.
17. Bullnheimer B, Hartl RF, Strauss C. A new rank-based version of the ant system, *a computational study, Technical Report POM-03/97*, Institute of Management Science, University of Vienna, 1997.
18. Steven G, Querin O, Xie M. Evolutionary structural optimization (ESO) for combined topology and size optimization of discrete structures, *Comp Meth Appl Mech Eng* 2000; **188**: 743-54.
19. Pitakaso R, Almeder C, Doerner KF, Hartl RF. A max-min ant system for unconstrained multi-level lot-sizing problems. *Comput Oper Res* 2007; **34**: 2533-52.
20. Atkinso G, Beresnev I. Compatible ground motion time histories for new national seismic hazard maps, *Can J Civ Eng* 1998; **25**: 305-18.
21. Shinozuka M, Sato Y. Simulation of nonstationary random processes, *J Eng Mech, ASCE* 1967; **93**(1): 11-40.
22. Jennings PC, Housner GW, Tasi NC. Simulated earthquake motions report, *Earthquake engineering research laboratory, Calif Inst Technol*, 1968.
23. Moller O, Foschi RO, Rubinstein M, Quiroz L. Seismic structural reliability using different nonlinear dynamic response surface approximations, *Struct Saf* 2009; **31**: 432-42.
24. Yang J, Li JB, Lin G. A simple approach to integration of acceleration data for dynamic soil–structure interaction analysis, *Soil Dyn Earthq Eng* 2006; **26**: 725-34.
25. Code of Practice for Skeletal Steel Space Structures, No. 400, 2010, http://tec.mporg.ir.
26. Fadaee MJ, Salajegheh E, Salajegheh J, Mashayekhi M. Reliability-based Topology Optimisation of Space Structures using Ant Colony Optimisation. *Proceedings of the Tenth International Conference on Computational Structures Technology*, BHV Topping, JM Adam, FJ Pallarés, RBru and ML Romero, (Eds), Civil-Comp Press, Scotland, 2010.